
Water discharge variations control fluvial stratigraphic architecture in the middle Eocene Escanilla formation, Spain

Nikhil Sharma[1], Alexander C. Whittaker[2], Stephen E. Watkins[1], Luis Valero[1,3], Jean Vérité[4], Cai Puigdefabregas[5], Thierry Adatte[6], Miguel Garcés[5,7], François Guillocheau[8], Sébastien Castelltort[1]

[1]University of Geneva, Department of Earth Sciences, Rue des Maraichers 13, 1205 Geneva, Switzerland

[2]Department of Earth Science and Engineering, Imperial College London, South Kensington, London SW7 2AZ, England

[3]Paleomagnetic Laboratory CCiTUB-Geo3Bcn, Geosciences Barcelona–CSIC, C/Lluis Solé i Sabarís s/n, 08028 Barcelona, Spain

[4]LPG – Le Mans, UFR Sciences et Techniques, Université du Maine, 72089 Le Mans cedex 9, France

[5]Department of Earth and Ocean Dynamics, Faculty of Earth Sciences, Universitat de Barcelona, C/ Martí I Franquès, s/n, 08028 Barcelona, Spain

[6]Institute of Earth Sciences (ISTE), University of Lausanne, Bâtiment Géopolis, 1015 Lausanne, Switzerland

[7]UB-Geomodels Research Institute, Universitat de Barcelona, 08028 Barcelona, Spain

[8]Géosciences Rennes, Campus de Beaulieu, Université de Rennes 1, 35042 Rennes cedex, France

ABSTRACT

Ancient fluvial deposits typically display repetitive changes in their depositional architecture such as alternating intervals of laterally-stacked, high-amalgamation (HA) channels, and floodplain-dominated intervals with vertically-stacked, low-amalgamation (LA) channels. Such patterns are usually ascribed to slow and high rates of base-level rise respectively, but "upstream" factors such as water discharge and sediment flux have also been recognized for their potential role in controlling stratigraphic architecture but have not been tested in ancient fluvial systems. Here, we use palaeohydraulic reconstructions to document riverbed gradient evolution within three middle Eocene (~40 Ma) fluvial HA-LA sequences in the Escanilla formation in the south-Pyrenean foreland basin. We show, in an ancient fluvial system, that river slope was primarily driven by climate-controlled water discharge variations rather than base-level changes as commonly assumed. These results have fundamental implications for the interpretation of the fluvial stratigraphic record and for our ability to reconstruct ancient hydroclimates.

INTRODUCTION

An assemblage of fluvial deposits such as vertically stacked isolated channels and laterally extensive amalgamated channels reflects the complex interplay of various factors such as climate, tectonics, and base-level fluctuations [Dalrymple et al 1998; Hajek et al. 2010; Straub et al. 2020]. In theory, both "downstream" i.e., base-level changes which in its simplest form is relative sea level and represents the joint effect of eustasy and tectonics (local subsidence rates), or a stratigraphic reference level above which sub-aerial erosion prevails [Schumm 1993], and "upstream" factors i.e., sediment flux, sediment size, and water discharge, have been recognised for their ability to determine patterns of channel-floodplain sequential arrangements [Wright & Marriot 1993; Shanley & McCabe 1994; Heller & Paola 1996; Gibling et al. 2011; Hajek et al. 2012; Armitage et al. 2015]. For instance, in the downstream sectors of a fluvial system, the historical approach involving stratigraphic base-level [Wright & Marriott 1993; Shanley & McCabe 1994; Dalrymple et al. 1998; Posamentier & Vail 1988] considers the interplay of two rates – the rate of change of accommodation space, hereafter referred to as ‘A’, i.e., the space available for sedimentation and the rate of sediment supply, hereafter referred to as ‘S_d’, and the resulting balance in the form of ‘A/ S_d’ as the predominant factor controlling sediment depositional architecture [Schlager, W. 1993]. In practice, changes in the stacking pattern of conglomerates and sandstone are often interpreted as changes in A/ S_d (Fig. 1a) with laterally stacked strata interpreted as being deposited under low A/ S_d (High Amalgamation (HA) intervals) while vertically stacked strata are interpreted as being deposited under high A/ S_d (Low Amalgamation (LA) intervals) [Armitage et al. 2015]. Similarly, Wright & Marriott (1993) in their sequence stratigraphic model proposed the deposition of multistorey sand bodies under low ‘A’ while vertically stacked isolated channels encased into thick floodplain deposits would form during periods of increasing ‘A’. Although the role of ‘S_d’ in sequence stratigraphy has now been better acknowledged [Catuneanu et al. 2009], sequence stratigraphic interpretations are often based on the primacy of base-level controlled ‘A’, due to the inherent difficulties in reconstructing ‘S_d’ [Martinius et al. 2014].

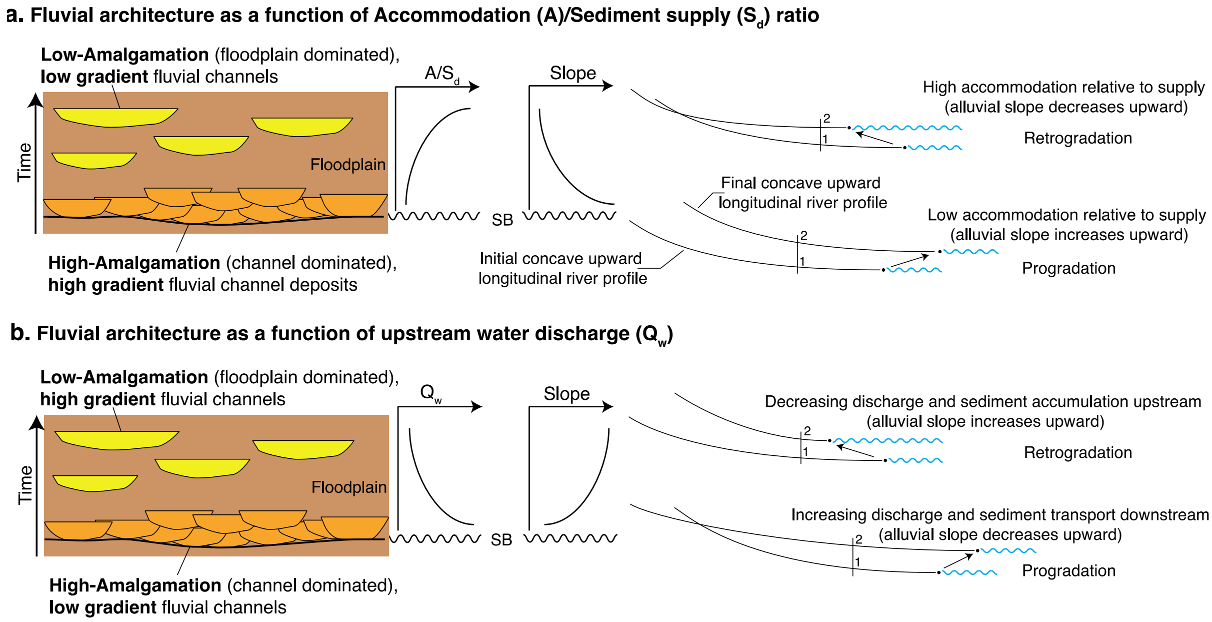

Fig 1 **Conceptual figure explaining fluvial architecture as a function of the Accommodation (A) to Sediment supply (S_d) ratio and water discharge (Q_w). a.** Low A/ S_d results in the deposition of high gradient fluvial channels with a high degree of amalgamation and an overall progradation of the system. Under high A/ S_d, low gradient fluvial channels with a low degree of amalgamation are deposited with an overall retrogradation of the system **b.** As Q_w increases, low gradient channels with a high degree of amalgamation are deposited with an overall progradation of the system while as Q_w decreases, high gradient channels with a low degree of amalgamation are deposited with an overall retrogradation of the system. Although there is rising base-level in this scenario, it is primarily driven by the differential rates in local subsidence.

While many historical approaches consider downstream factors fundamental in controlling the long profile and sedimentary record of alluvial rivers, several studies [Blum 1993; Shanley & McCabe 1994; Holbrook et al. 2006; Wang et al. 2020] have demonstrated that upstream factors have an influence over much of the river profile. For alluvial rivers, where base level variations are not the only dominant control on creation of 'A', one must consider the resulting equilibrium profile [Dalrymple et al. 1998]. For instance, the early work of fluvial geomorphologists such as Lane (1955) and Leopold & Bull (1979) has indicated that the equilibrium river profile and thus channel slope is a function of upstream boundary conditions of sediment flux, sediment size, and water discharge. Experimental studies such as numerical modelling and sedimentary forward modelling studies too have recognised the role of upstream factors in modifying the river profile [Sun, Paola, Parker, & Meakin, 2002; Van den Berg Saparoea & Postma, 2008; Simpson and Castelltort 2012; Wang et al. 2020]. Through a series of numerical experiments, Simpson and Castelltort (2012) highlighted the evolution in slope of a river profile under sinusoidal water flux variations such that river profile gradient increases as water flux decreases and the gradient decreases as water discharge increases. In terms of stratigraphic architecture, this could be seen as low gradient higher amalgamation "HA" intervals being deposited under high water discharge while higher gradient lower amalgamation "LA" intervals are deposited under low water discharge (Fig. 1b). Field based studies in the past [Olsen 1990, 1994] have documented water discharge variations under orbital forcing parameters as the primary control on varying thicknesses of fining upward sequences in the Devonian-aged fluvial section from East Greenland, while more recent studies such as Noorbergen et al. (2020) have pointed at enhanced discharge and sediment supply during seasonal conditions under increasing eccentricity in affecting fluvial architecture and sedimentation patterns in continental settings [Noorbergen et al. 2020].

Channel slope evolution in this framework depends on whether the sequences are 'A' controlled or 'S_d' controlled. In 'A' controlled sequences, the "LA" stacking pattern has lower slope while the "HA" stacking pattern has higher slope (Fig. 1a). 'S_d' controlled sequences on the other hand have "LA" intervals with higher slope while "HA" intervals have lower slope (Fig. 1b). Channel slope evolution may thus be seen as a potential diagnostic tool to distinguish between upstream palaeo-environmental drivers on the stratigraphic record relative to a base level control. An outstanding research challenge in this field, therefore, lies in deciphering the factors controlling these changes in observed fluvial architecture at a range of temporal and spatial scales. Field-based work such as Foreman et al. (2012) and Lyster et al. (2021) along with empirical studies based on flume experiments and modern river systems [Leclair & Bridge 2001; Trampush et al. 2014] have demonstrated the ability to meaningfully quantify palaeohydrological parameters, including channel gradients, from the rock record. These include the development of tools to estimate palaeoslope [Paola & Mohrig 1996; Trampush et al. 2014], and other palaeohydrological parameters such as flow velocity, water discharge and sediment flux.

Yet, to our knowledge, the evolution of river slope across fluvial sequences in relation to documented cyclical changes in stratigraphic architecture has never been explored at high resolution. In this work, we address this problem using the well-documented middle Eocene Escanilla formation in Spain [Kjemperud et al. 2004; Labourdette & Jones 2007; Labourdette 2011] as an exceptional natural laboratory to explore the drivers of such cyclicity and the environmental factors they record. We estimate channel slope evolution, along with estimating channel-belt widths and identifying channel-belt style (sheet or ribbon), flow velocity, water discharge and sediment flux, across several stratigraphic cycles, each containing a "HA" and "LA" interval (Fig. 3). Our palaeohydraulic estimates show a systematic increase in discharge and sedimentary fluxes during "HA" intervals, thereby pointing towards upstream driven climate control that we discuss in relation to the Earth's orbital cycles.

The Escanilla sediment routing system as a natural laboratory. The Escanilla system is an ancient sediment routing system of late Lutetian to late Priabonian age, approximately 42 - 36 Ma, and deposited in the south-Pyrenean foreland basin, Spain [Bentham & Burbank 1996]. The Escanilla formation was mainly sourced from the Pyrenean central massif through large valleys filled with transverse alluvial fans, such as the fan system of the Sis palaeovalley [Allen et al. 2013] and the Gurb escarpment [Michael et al. 2014] further east (Fig. 2a). The maximum preserved thickness of the Escanilla formation within the Ainsa basin is approximately 1000 m [Labourdette & Jones 2007], and is subdivided into two informal members, the Mondot and Olson members [Dreyer 1993] with a basin-wide extending conglomeratic channel-complex, here named the 'Olson sheet' at the transition between the two members (Fig. 2b, 2c). Kjemperud et al. (2004) subdivided the Escanilla formation into three units based on changes in alluvial geometry which are further subdivided into seven unconformity bound sequences. Similar alternating sequences have also been identified by [Labourdette & Jones 2007; Labourdette 2011] as basin-wide, laterally extensive amalgamated channels and vertically stacked isolated channels. We focus on exposures near Olson, where the gullied landscape and exceptional outcrop preservation allow a detailed documentation of stratigraphic architectural changes across three sequences, which correspond to sequencess 2, 3 and 4 by Kjemperud et al. (2004) and sequences 1, 2 and 3 by Labourdette & Jones (2007) and Labourdette (2011). Based on the local magnetostratigraphy, the studied sequences represent a few hundred thousand years of deposition at approximately 40 Ma (Fig. 2c).

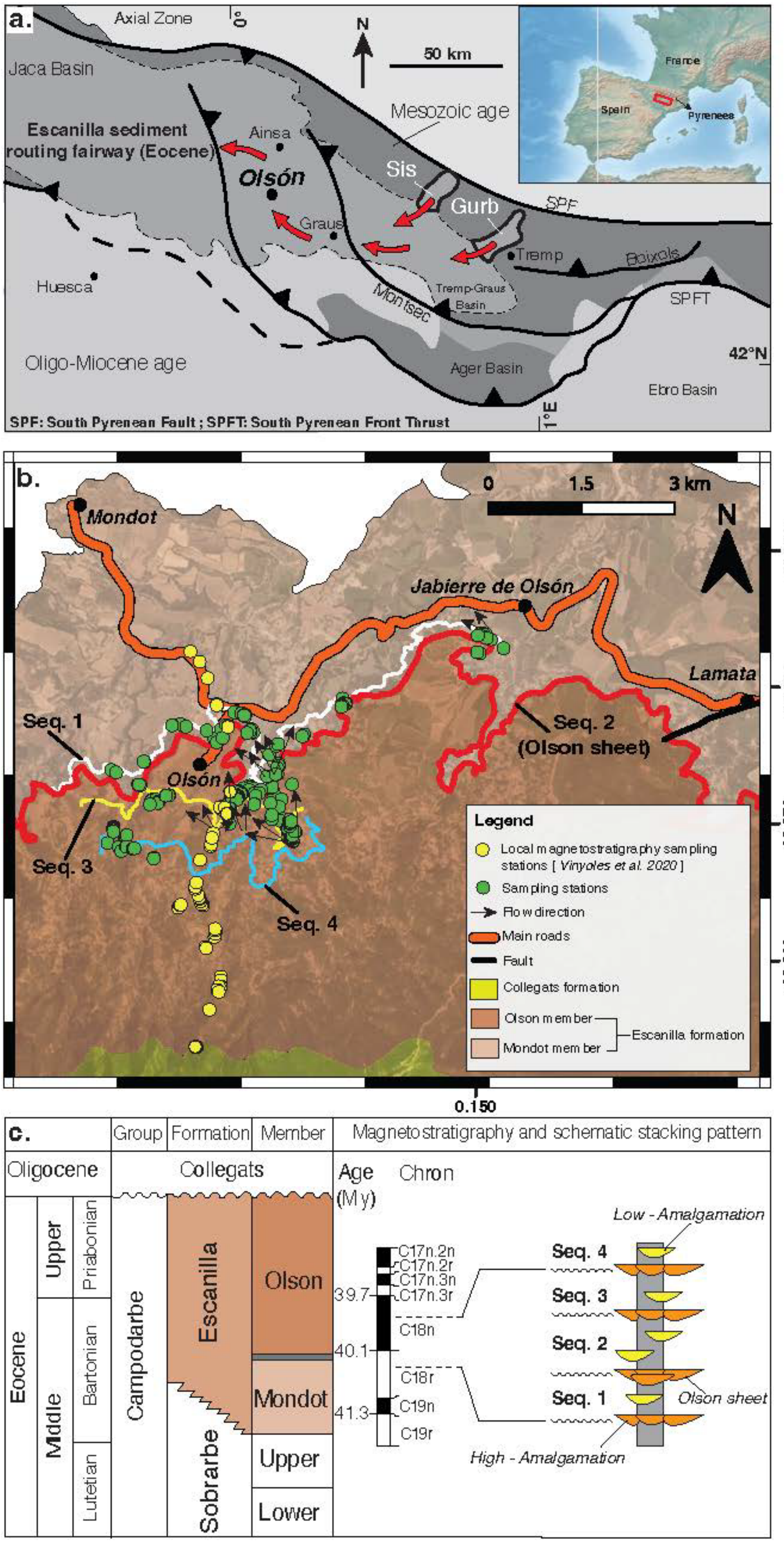

Fig 2 **Geological setting of the Escanilla sediment routing system and the Escanilla formation at Olson. a.** Geological setting of the south-Pyrenean Foreland basin containing the Escanilla sediment routing fairway. Red

arrows mark the sediment transport direction of the Escanilla system from the source regions of Sis and Gurb. Map modified from Kjemperud et al. (2004) **b.** Geological map of the southern Ainsa basin encompassing the Escanilla formation around the village of Olson where the study area lies. Sampling stations are displayed along with flow directions with respect to the sampled sequences. The 'Olson sheet' is marked in red as a basin wide, laterally extensive amalgamated channel body lying in-between the Mondot and Olson members of the Escanilla formation. **c.** Lithostratigraphic framework [Bentham et al. 1992; 1993] of the Escanilla formation at Olson consists of two main members – the Mondot and Olson member with the 'Olson sheet' lying at the transition between the two members. Also displayed is the magnetostratigraphic correlation [Vinyoles et al. 2020] and the schematic stacking pattern along the studied section. It is noteworthy that the thickest normal magnetozone represents Chron C18n, which includes C18n.1n+C18n.1r+C18.2n (the very short C18n.1r is missing).

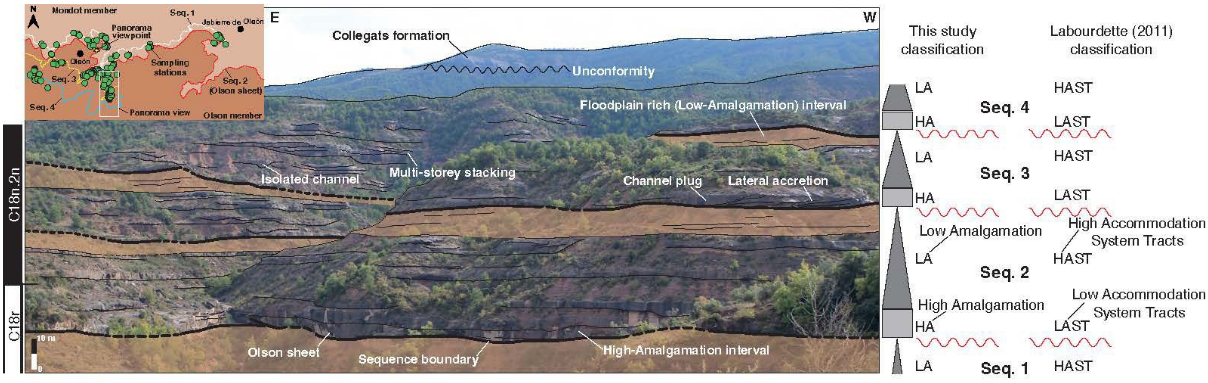

Fig. 3 **Panorama depicting the studied sequences containing High-Amalgamation (HA) and Low-Amalgamation (LA) intervals.** This panorama depicts the studied sequences 2, 3 and 4. Note that sequence 1 lies below the photographed interval and could not be captured. At the base of the panorama lies a thick floodplain rich interval above which lies a High-Amalgamation (HA) interval containing the 'Olson sheet' and separated by a sequence boundary. Above the HA interval lies the floodplain dominated Low-Amalgamation (LA) interval. Several stratigraphic features such as channel plug, lateral accretion, isolated channel, and multistorey stacking pattern have been marked as well. To the top of the panorama lies the Oligocene aged Collegats formation separated from the underlying Escanilla formation by an unconformity. An inset map has also been provided to make it easier for the reader to locate themselves along with a timescale marking the age of the photographed interval to the left of it. On the extreme right, the High-Amalgamation (HA) and Low-Amalgamation (LA) classification used in this study is compared to the High Accommodation System Tracts (HAST) and Low Accommodation Systems Tracts (LAST) classification used by Labourdette (2011).

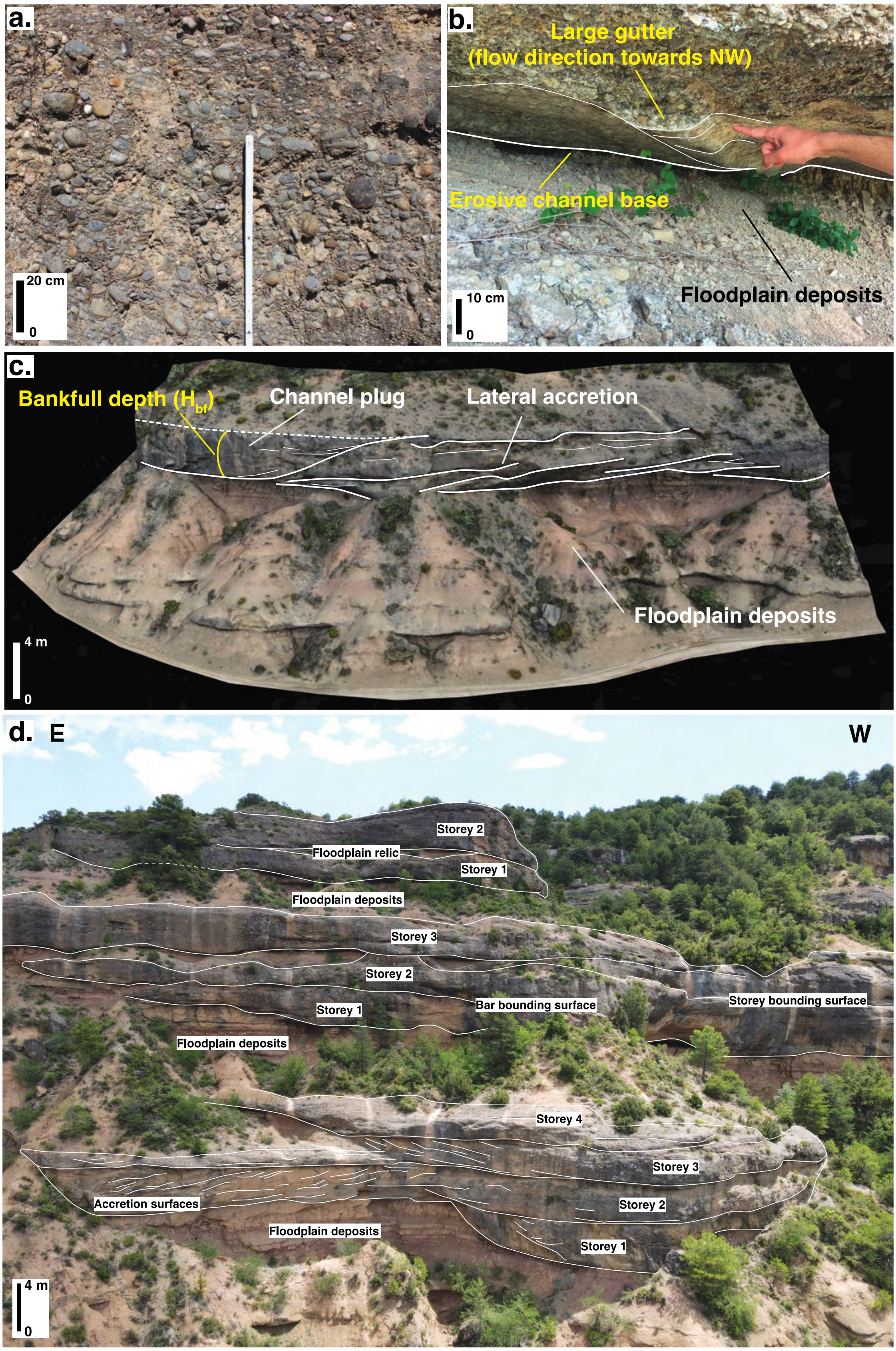

Fig. 4 **Outcrop photographs. a.** Channel basal gravel from which grain size estimates are obtained. **b**. A large gutter used to reconstruct flow direction. It is marked as a long tube-like feature at the level of the erosive

channel base lying over floodplain deposits **c.** A 3D model of an outcrop containing a channel plug and lateral accretion deposits, which illustrate the stratigraphic expression of H_{bf} **d.** Multi-storey stacking pattern observed in the Low Amalgamation (LA) interval of sequence 4. Several different stratigraphic features such as the different stories, accretion surfaces, storey bounding surface, bar bounding surface and floodplain relic are marked.

RESULTS

Grain size, bankfull depth and palaeoslope evolution. We measured the coarse grain size fraction (> 4 mm) (methods, Fig. 5) at 180 stations distributed across the study interval. We find that the coarse grain size fraction in channel bodies has a range of grain sizes from 6 ± 2 [mm] to 30 ± 2 [mm] over the studied interval (Fig. 5), indicating a clear variation in the calibre of material supplied to the system. At the scale of individual sequences, ”HA” intervals have a grain size of 19 ± 1 [mm] (average value ± standard error, N = 77), while ”LA” intervals have a grain size of 17 ± 1 [mm] (N = 103), indicating that channel body grain size is only 2 mm (~10%) larger in channels with a high degree of amalgamation. Although relatively small, this difference is nevertheless statistically significant at the 95% confidence level (t-value = 2.98, p-value = .003, power = 0.91, dof = 178). It is noteworthy that the bulk grain size of ”LA” intervals is significantly lower due to the greater preservation of fine-grained floodplain material (50 – 70 % of “LA” intervals).

Bankfull depths based on preserved storey thickness (methods, Fig. 5) reveal a trend of higher depths in the ”HA” intervals and substantial decrease in the ”LA” intervals. ”HA” intervals have depths of 5.0 ± 0.4 [m] (average value ± standard error, N = 45) while ”LA” intervals have depths of 3.5 ± 0.3 [m] (N = 49), i.e., an increase of 40 % during deposition of the ”HA” intervals. These field observations suggest that the palaeohydrology of channels comprising the ”HA” and ”LA” intervals is not the same. A t-test on bankfull depth data rejects the null hypotheses that ”HA” and ”LA” intervals have the same average values at the 95% confidence level (t-value = 6.83, p-value = $.8e^{-9}$, power = 0.67, dof = 92).

Our palaeoslope estimates, obtained using the equation proposed by Trampush et al. (2014) (equation (1), are consistently lower in the ”HA” intervals and markedly increase into the ”LA” intervals (Fig. 5). Palaeoslope estimates based on averaged field grain size and channel depth data of 7 storeys within “HA” stratigraphic intervals (77 grain size sampling stations wherein 100 – 200 clasts were counted per station, and 45 channel depth estimates) have a palaeoslope of $5 \times 10^{-4} \pm 5 \times 10^{-5}$ [m/m] (average value ± standard error, N = 7), equivalent to 0.03°, while 11 storeys within “LA” stratigraphic intervals (103 grain size sampling stations and 49 channel depth estimates) have a palaeoslope of $8 \times 10^{-4} \pm 6 \times 10^{-5}$ [m/m] (N = 11), equivalent to 0.05°, and representing a 60% increase in slope in the ”LA” interval. A t-test on palaeoslope estimates (t-value = -4.02, p-value = .001, power = 0.16, dof = 15) rejects the null hypotheses that ”HA” and ”LA” intervals have the same average values at the 95% confidence level. Although absolute palaeoslope values are different when using other palaeoslope estimators such as the Shields stress inversion approach [Paola and Mohrig, 1996], they nevertheless give similar trends (supplementary material Fig. 1).

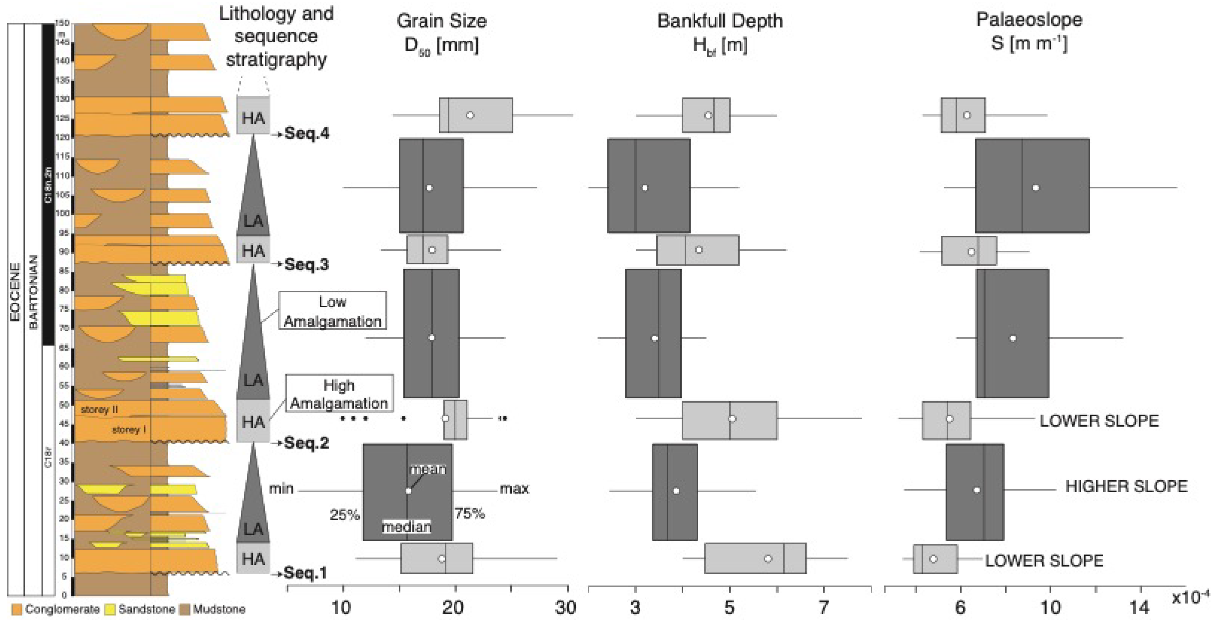

Fig. 5 **Grain-size, flow depth and palaeoslope evolution.** Stratigraphic log of the studied section depicting three fining upward sequences, each containing a High-Amalgamation (HA) interval at the base overlain by a floodplain dominated Low-Amalgamation (LA) interval. The stratigraphic log has been correlated to the geomagnetic polarity timescale 2016 [Vinyoles et al. 2020; Ogg et al. 2016]. At the right of the log are shown the grain size, D_{50} [mm] evolution across the section followed by the bankfull depth, H_{bf} [m] and finally the palaeoslope, S [m/m] estimates.

Channel-belt width estimates and channel body geometry. Channel-belt widths are crucial in estimating total discharge and flux, e.g., the recent work of Greenberg et al. (2021) and Lyster et al. (2021). Despite the excellent outcrop conditions in our study area, fully preserved channel cross-sections required to measure width in the field, are nevertheless rarely preserved. To circumvent this limitation, we estimate channel-belt widths using the relationship proposed by Bridge & Mackey (1993) which is based on modifications proposed to the computer simulation model of Bridge & Leeder (1979) (methods and supplementary material Fig. 3) and compare them to width measurements of channel plug and lateral accretion deposits where preserved (supplementary material Fig. 2). Our results suggest that "HA" channel-belts are typically twice wider, 171 ± 22 [m] (average value ± standard error, N

= 45) than “LA” channel belts, 86 ± 11 [m] (N = 49). A comparison to width and depth of modern rivers having similar grain size (5 mm to 45 mm) and flow depth (2 m to 7.5 m) (Fig. 6) suggests active flow widths within ”HA” channel belts were more likely near a central value of 180 meters, in a range of 60 m to 400 m while ”LA” channel belts were more likely near a central value of 90 meters, in a range of 30 m to 200 m. These are less than the “geobody” widths estimated by Labourdette & Jones (2007) and so represent conservative values. A cross plot between depth and width estimates implies more sheet-like channel geometry during ”HA” intervals while ”LA” intervals have a more ribbon-like channel geometry (Fig. 6).

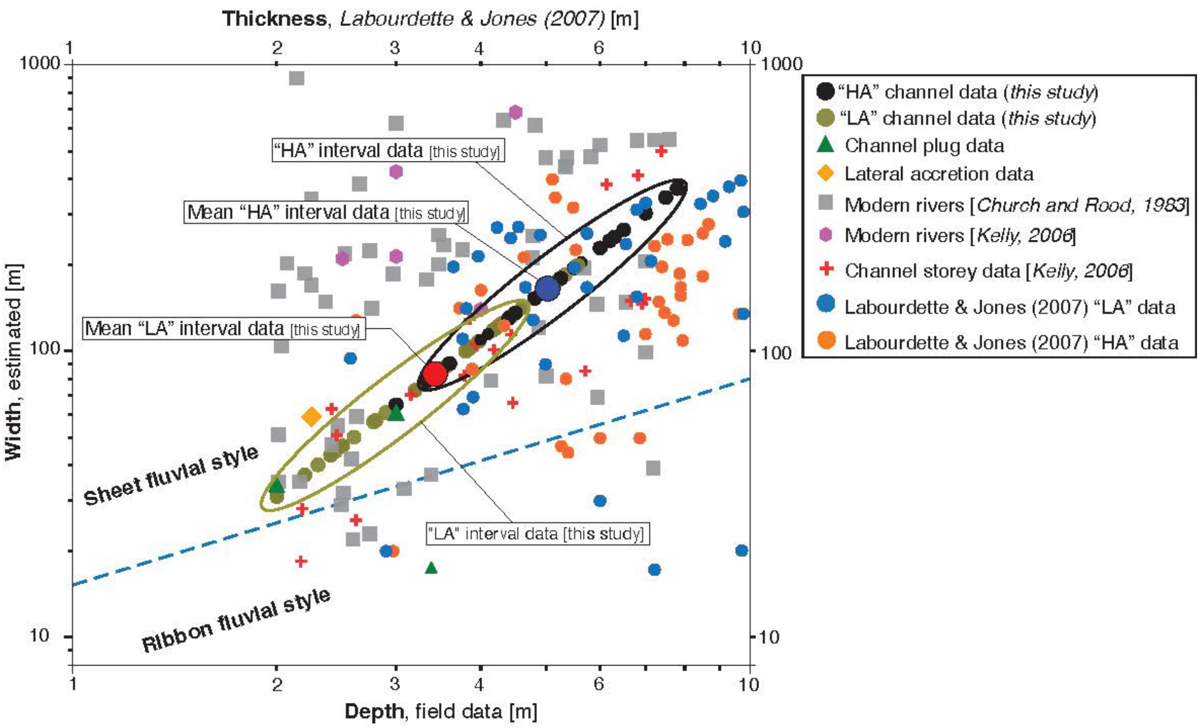

Fig. 6 **Comparison of modern river channel width and depth to estimates from this study.** Modern river data collected from the Church and Rood (1983) catalogue and Kelly (2006). A range of possible widths is obtained for rivers having similar flow depths allowing us to estimate the uncertainty on our estimated widths. Comparisons are also made to field measurements from this study and storey data by Kelly (2006). A prediction of the fluvial style of the High Amalgamation (HA) and Low Amalgamation (LA) channels is also made.

Hydrodynamics and sediment transport. Plausible flow velocities, deduced across all field data using Manning’s equation (equation (2)), have an average value (± standard error) of 2.1

± 0.4 [m s^{-1}] (N = 94) (supplementary material, Fig. 3). Multiplying flow velocity by estimated depths, we estimate unit discharge in ”HA” intervals to be 11 ± 2 [m^2 s^{-1}] (mean value ± standard error, N = 45) and 7 ± 1 [m^2 s^{-1}] (N = 49) in ”LA” intervals (supplementary material Fig. 4). Multiplying unit discharge by channel-belt width estimates would imply a total discharge rate of 2200 ± 550 [m^3 s^{-1}] (average value ± standard error, N = 45) in ”HA” intervals, and a discharge rate of 700 ± 200 [m^3 s^{-1}] (N = 49) in the ”LA” intervals (Fig. 7; equation (3)). This amounts to a 3-fold increase of volumetric channel-forming discharge during “HA” intervals. We obtain conservative discharge estimates when using channel plug and lateral accretion width estimates such that ”HA” intervals have discharge rates of 700 ± 150 [m^3 s^{-1}] (average value ± standard error, N = 45) while ”LA” intervals have a total discharge of 200 ± 50 [m^3 s^{-1}] (N = 49). Nevertheless, the cyclical pattern of higher discharge rates in “HA” intervals and lower discharge rates in “LA” intervals does not change upon using the different width estimates (Supplementary material Fig. 5).

Unit bedload sediment flux estimated using the Meyer-Peter and Muller equation (equation (4)), is estimated to be 1.7 ± 0.2 [kg m^{-1} s^{-1}] (average value ± standard error, N = 45) and 2.0 ± 0.1 [kg m^{-1} s^{-1}] (N = 49) for ”HA” and ”LA” intervals respectively (supplementary material Fig. 4). Multiplying unit flux by channel-belt width estimates would imply total sediment flux (equation (4)) for ”HA” intervals to be at 300 ± 50 [kg s^{-1}] (average value ± standard error, N = 45), equivalent to 0.3 ± 0.05 [m^3 s^{-1}], and for ”LA” intervals to be at 200 ± 20 [kg s^{-1}] (N = 49), equivalent to 0.2 ± 0.02 [m^3 s^{-1}], i.e., a 1.5-fold increase in bedload sediment flux during ”HA” intervals (Fig. 7). When considering the additional preservation of floodplain material during ”LA” intervals compared to ”HA”, the results above predict a marked increase in the export of clastic material out of the Escanilla fluvial system during ”HA” intervals.

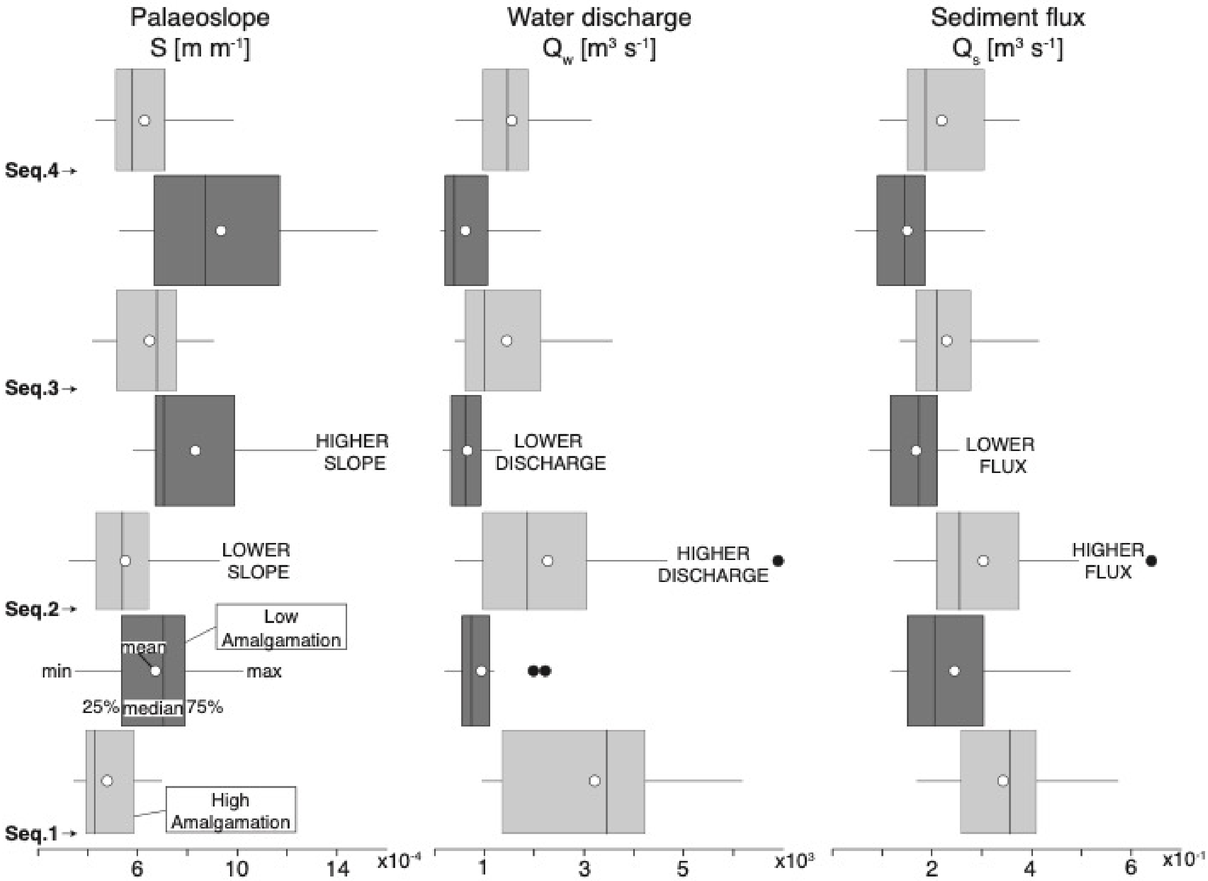

Fig. 7 **Palaeoslope, total water discharge and total bedload sediment flux estimates.** Sequence wise palaeoslope evolution have been shown along with estimates of water discharge and bedload sediment flux. It is important to note the relationship and cyclical pattern between the three parameters such that river slope is lower when discharge and flux are higher while river slopes are higher when discharge and flux are lower.

DISCUSSION

Our results provide new insights into how palaeoslopes and palaeohydrology of the middle Eocene Escanilla system evolved during transitions between "HA" and "LA" type channel architecture. Importantly, palaeoslopes vary in relation to total water discharge and total bedload sediment flux such that palaeoslopes increase into the "LA" interval where a decrease in total discharge and total sediment flux is documented. The opposite is true for "HA" intervals wherein lower palaeoslopes correspond to higher water discharge rates and sediment flux. Notably, unit discharges (supplementary material Fig. 5) are not constant in time and document an increase in "HA" intervals which substantially decreases into the "LA" interval. Since unit discharges are width independent, our results highlight the role of upstream factors in modulating water discharge variations.

Upstream forcing can be either due to tectonic (10^6 – 10^8 years) or climatic changes (10^3 – 10^6 years), which are the two allogenic factors primarily influencing depositional systems in the continental domain [Armitage et al. 2011; Tofelde et al. 2019]. Although these two factors influence sediment flux, tectonic activity mainly influences sediment flux without altering water discharge unless the drainage network is affected. Climatic changes on the other hand primarily affect water discharge along with a change in the sediment volume and grain size due to a modification of the sediment transport capacity [Romans et al. 2016; Tofelde et al. 2019]. The main driver of accommodation space is often attributed to basin subsidence and/or hinterland uplift [Fisher et al. 2013]. For example, the vertical trends in stratigraphic arrangement at Olson could be the result of tectonic movements in the Ainsa piggy-back basin [Labourdette & Jones 2007], although these would have had to have taken place over timescales of 10^5 years to explain the stacking patterns observed (Fig. 2c). Variations in climate on the other hand are known to have a significant impact on fluvial architecture due to variations in water discharge, sediment supply, and sediment size [Parrish 1998; Blum & Tornqvist 2000; Bridge 2003; Allen et al. 2014]. Climatic fluctuations between wetter and dryer periods control variation in water discharge and thus the competence of rivers and the sediment calibre. Climatic changes also influence the volume of sediments produced and released from the hinterland area [Leeder et al. 1998; Densmore et al. 2007; Armitage et al. 2011]. Thus, a better explanation for the fining upward trend of each sequence is as a result of decreased precipitation and sediment discharge from the catchment areas supply to the study area. A change in palaeoslope and discharge from "HA" to "LA" intervals therefore implies that these rivers were responding to changes in climate in the hinterland region. Since the cyclical trend of the three fining upward sequences indicates a recurrence of pattern of the controlling factor(s), our finding of cyclical variations in water discharge and sediment flux implies that climate cyclicity is the main driver of stratigraphic architecture in the Escanilla formation at Olson. Our conclusion of climate influence is consistent with the findings of a numerical modelling study [Armitage et al. 2015] on the Escanilla sediment routing system, which predicted increased sediment flux due to increased precipitation in the catchment area during the Middle Eocene Climatic Optimum (MECO), approximately around 40 Ma, an enigmatic global warming event that lasted for around 500 kyr [Sluijs et al. 2013].

What drove climate variations? Several outcrop studies in the Spanish Pyrenees have pointed to Milankovitch cyclicity as an important factor controlling depositional processes [Cantalejo et al. 2020]. For instance, a cyclo-stratigraphic study in the Eocene marine deltaic rocks, coeval with the Escanilla formation, deposited in the Jaca Basin proposed orbitally induced changes in magnetite content due to increased terrigenous input delivered by a fluvial source during periods of increased precipitation at times of eccentricity maxima [Kodama et al. 2010]. Orbital changes have also been shown to influence depositional style through control on siliciclastic sediment supply to the deep-marine Ainsa basin [Heard et al. 2008; Cantalejo & Pickering 2014, 2015]. To explain our marked changes in discharge from the "HA" to "LA" intervals, we hypothesise that eccentricity-modulated water discharge variations to in-turn drive palaeoslope changes from "HA" to "LA" intervals. This is based upon the physical rationale that in general, eccentricity maxima promote the largest precession/insolation amplitudes which are more likely to trigger intense, extreme events (either wet or dry) [Zeebe et al. 2017]. This would result in increased mobilization of sediments due to high weathering rates in the source area and enhanced transport of coarser sediments (higher D_{50}) and/or higher water depths. Contrary to this, eccentricity minima are periods of low seasonality with rather stable climates [Cheng et al. 2016].

Implications and conclusion. Our findings have several fundamental implications for classical sequence stratigraphic predictions, sedimentary landscape evolution over geological timescales, the prediction of ancient hydroclimates during greenhouse forcing, and for industrial applications in resource exploration. Firstly, our findings illustrate the dominant role of sediment supply (i.e., 'S_d' in 'A/ S_d') and the resulting stratigraphic architecture instead of the dominant role of 'A' as is often assumed [Wright & Marriott 1993; Shanley & McCabe 1994]. Secondly, our results support the prediction of higher sediment flux during "HA" intervals. This is in excellent agreement with sequence stratigraphic predictions in which "HA" intervals are formed during low A/ S_d (base-level fall) and thus greater transport of sediments to the deep sea and marine environments. This work is also fundamental for our ability to reconstruct ancient hydroclimates from the sedimentary record and compare it to numerical model predicted response of the hydrologic cycle to warming conditions. For instance, modelling studies of the Palaeocene-Eocene Thermal Maximum (PETM) have suggested an intensification of the hydrological cycle on a global scale in response to greenhouse gas levels [Rush et al. 2021]. Our results are also consistent with the findings of Barefoot et al. (2021) where high discharge variations during the hyperthermal PETM increased channel mobility. During the middle Eocene greenhouse conditions, "HA" intervals therefore represent periods of increased channel mobility under increasing water discharge rates while "LA" intervals represent low channel mobility under decreasing water discharge rates.

Our framework of palaeoslope and palaeohydrological reconstruction across three fining upward sequences in the middle Eocene aged Escanilla formation, for the first-time, documents lower river slope during higher water discharge and sedimentary flux with the deposition of river channels having a high degree of amalgamation, and higher slope during lower water discharge and sedimentary flux with the deposition of river channels having a low degree of amalgamation. The studied fining upward sequences together with our finding of cyclic variations in water discharge and sediment flux represents a major paradigm shift by suggesting climate may have controlled the entire sedimentary landscape evolution during the middle Eocene greenhouse conditions instead of eustatic variations, and with palaeohydraulic reconstructions to test different options without the need of an independent eustatic curve.

METHODS

Field observations. We focus on 3 fining upward sequences. Each fining upwards sequence consists of a thick and laterally extensive channel-dominated High-Amalgamation (HA) interval at the base, above which lies a much thinner, less laterally extensive floodplain-dominated Low-Amalgamation (LA) interval which progressively thins towards the top of the sequence. The thickness of each such fining upward sequence is 35-45 m.

Data collection. Palaeohydrological field data were collected from channel fill deposits particularly channel basal gravels for grain size distribution and storey thicknesses as flow depth estimates. This data along with uncertainties associated with individual measurements were propagated through a quantitative framework to reconstruct hydrological parameters such as flow depths, palaeoslope, flow velocities, water discharge rates, bedload sediment flux.

Grain size measurements were collected using the Wolman sampling procedure [Wolman 1954]. The longest axis was measured as a proxy for the intermediate b axis on 100 - 200 grains per sampling station. The procedure was performed on photographs taken with a Canon EOS 2000D camera of 24.1Mpixels resolution on an outcrop area of 1 x 1 m^2. Grains were measured at the nodal intersection of a virtual grid such that a repeat count of grains is avoided. Measurements were made using ImageJ2 version 2.3.0/1.53f. The data obtained is normalized using the (psi) scale, a logarithmic scale with base two, to perform statistical analyses and obtain the 50th percentile (D_{50}) of the grain size distribution.

Flow depth estimates are based on preserved storey thicknesses, channel-plug, and bar-scale clinoform heights measured using a laser range finder (TruPulse model 200) and following the procedure outlined in Mohrig et al. (2000) and Kelly (2006). It is important to note that while preserved thicknesses are lower than the original flow depths, preserved thicknesses do not severely underestimate the original depth [Paola & Borgmann 1991; Paola & Mohrig 1996].

Quantitative paleohydrology. Palaeoslopes were estimated using the empirical equation proposed by Trampush et al. (2014) (equation (1)). We use this equation as our grain size measurements in a few instances are less than the 8 mm threshold required to use the Shields stress inversion approach [Paola and Mohrig 1996].

$$logS = \alpha_0 + \alpha_1 \, log \, D_{50} + \alpha_2 \, log \, H_{bf} \tag{1}$$

It is an empirical equation, motivated by theoretical considerations, and provides a relationship between the channel slope (S), median grain size (D_{50}), and bankfull depth (H_{bf}). α_0, α_1 and α_2 are three empirical coefficients with values of -2.08 ± 0.0015 (mean ± standard error), 0.2540 ± 0.0007 and -1.0900 ± 0.0019, respectively. An average palaeoslope (± standard error) value has been estimated, per interval, using average median grain size values and average bankfull depths along with their respective standard errors. Average palaeoslope estimates are presented in [m/m], for example, a palaeoslope value of 0.001 represents aggradation of 1 m per 1000 m.

Channel-belt width W can be estimated using empirical scaling relations when direct measurements are not possible on the field. We estimate channel-belt widths using the relationship, $W = 8.8H_{bf}^{1.82}$ [Bridge & Mackey 1993]. Where possible, channel plug widths were estimated in the field using a laser range finder (TruPulse model 200) while widths from lateral accretion deposits was estimated using the procedure outlined in Greenberg et al. (2021).

Flow velocity, U was calculated using Manning's equation (equation (2)) where n = 0.03 ± 0.005 is the Manning's coefficient, R is the hydraulic radius approximated by channel flow depths and S is slope.

$$U = \frac{1}{n} R^{2/3} S^{1/2} \tag{2}$$

Total water discharge Q_w was calculated using equation (3)

$$Q_w = U \times H_{bf} \times W \tag{3}$$

For unit water discharge, W = 1.

Total bedload sediment flux Q_s was calculated using the Meyer-Peter and Muller equation (equation (4)).

$$Q_s = \rho_s \left(\Delta\rho g D_{50}^3\right)^{1/2} C(\tau^* - \tau_c^*)^{3/2} \times W \tag{4}$$

Where, $sediment\ density\ \rho_s = 2650\ kg/m^3$, buoyant density $\Delta\rho = 1.6$, constant $C = 8$, critical sheer stress τ_c^* = 0.047 and shear stress $\tau^* = \frac{H_{bf}S}{\Delta\rho D_{50}}$.

For unit bedload sediment flux, W = 1 and 1000 kilogram per second = 1 cubic meter per second.

Statistical tests. Uncertainty on results reported in this study consist of the standard error of the mean (SE) calculated as $SE = \frac{SD}{\sqrt{n}}$, where SD is the standard deviation and n is sample number. Uncertainty propagation was carried out using the uncertainties package on Python (Spyder version 4.0.1). Statistical analyses were performed on Python (Spyder version 4.0.1). To check for data normality, the Shapiro-Wilk test was performed using the *'scipy.stats.shapiro'* package. The null hypothesis that the data is normally distributed cannot be rejected when the p-value is greater than .05 at the 95% confidence level. To check for statistical significance, a two-sided t-test was performed for normally distributed data using the *'scipy.stats.ttest_ind'* package for the null hypothesis that two independent samples have an identical average value. For non-normally distributed data, a Kruskal-Wallis test was performed using the *'scs.kruskal'* package for the null hypothesis that the median value of all groups is similar. The null hypothesis can be rejected when the p-value is less than .05 at the 95% confidence level. The degree of freedom (dof) was estimated as '(nx+ny) – 2' where 'nx' and 'ny' are the lengths of the two independent parameters. Power analysis of t-tests was performed, using *'pingouin.power_ttest2n'*, to detect Type II errors. Pingouin is an open-source package written in Python 3 [Vallat 2018].

REFERENCES

1. Allen, J. P., Fielding, C. R., Gibling, M. R. & Rygel, M. C. Recognizing products of palaeoclimate fluctuation in the fluvial stratigraphic record: An example from the Pennsylvanian to Lower Permian of Cape Breton Island, Nova Scotia. *Sedimentology* **61**, 1332–1381 (2014).
2. Allen, P. A. *et al.* The Qs problem: Sediment volumetric balance of proximal foreland basin systems. *Sedimentology* **60**, 102–130 (2013).
3. Armitage, J. J. *et al.* Sediment Transport Model For the Eocene Escanilla Sediment-Routing System: Implications For the Uniqueness of Sequence Stratigraphic Architectures. *J Sediment Res.* **85**, 1510–1524 (2015).
4. Armitage, J. J., Duller, R. A., Whittaker, A. C. & Allen, P. A. Transformation of tectonic and climatic signals from source to sedimentary archive. *Nat Geosci* **4**, 231–235 (2011).
5. Barefoot, E. A. et al. Evidence for enhanced fluvial channel mobility and fine sediment export due to precipitation seasonality during the Paleocene-Eocene thermal maximum. *Geology* (2021).

6. Bentham, P. & Burbank, D.W. Chronology of Eocene foreland basin evolution along the western oblique margin of South-Central Pyrenees. In: Tertiary Basins of Spain: The Stratigraphic Record of Crustal Kinematics (*Cambridge University Press,* 1996).

7. Bentham, P. A., Burbank, D. W. & Puigdefabregas, C. Temporal and spatial controls on the alluvial architecture of an axial drainage system: late Eocene Escanilla Formation, southern Pyrenean foreland basin, Spain. *Basin Res* **4**, 335–352 (1992).

8. Bentham, P. A., Talling, P. J. & Burbank, D. W. Braided stream and flood-plain deposition in a rapidly aggrading basin: the Escanilla formation, Spanish Pyrenees. *Geological Soc. Lond. Special Publ.* **75**, 177–194 (1993).

9. Blum, M. D. & Tornqvist, T. E. Fluvial responses to climate and sea-level change: a review and look forward. *Sedimentology* **47**, 2–48 (2000).

10. Blum, M. D. Genesis and architecture of incised valley fill sequences: a late Quaternary example from the Colorado River, Gulf Coastal Plain of Texas, in Siliciclastic Sequence Stratigraphy: Recent Developments and Applications: *AAPG Memoir* **58**, 259-283 (1993).

11. Bridge, J.S. and Leeder, M.R. A simulation model of alluvial stratigraphy. *Sedimentology*, 26: 617-644. (1979).

12. Bridge, J.S. and Mackey, S.D. A Revised Alluvial Stratigraphy model. In Alluvial Sedimentation (*Wiley*, 1993).

13. Bridge, J.S. Rivers and Floodplains: Forms, Processes, and Sedimentary Record. Oxford: Blackwell, 491 pp (2003).

14. Cantalejo, B. & Pickering, K. T. Climate forcing of fine-grained deep-marine systems in an active tectonic setting: Middle Eocene, Ainsa Basin, Spanish Pyrenees. *Palaeogeogr. Palaeoclim. Palaeoecol.* **410**, 351–371 (2014).

15. Cantalejo, B. & Pickering, K. T. Orbital forcing as principal driver for fine-grained deep-marine siliciclastic sedimentation, Middle-Eocene Ainsa Basin, Spanish Pyrenees. *Palaeogeogr. Palaeoclim. Palaeoecol.* **421**, 24–47 (2015).

16. Cantalejo, B., Pickering, K. T., Miller, K. G. & Niocaill, C. M. Chasing the 400 kyr pacing of deep-marine sandy submarine fans: Middle Eocene Aínsa Basin, Spanish Pyrenees. *J. Geol. Soc. London* **178** (2021).
17. Catuneanu, O. et al. Towards the standardization of sequence stratigraphy. Earth-sci Rev **92**, 1–33 (2009).
18. Cheng, H., Edwards, R., Sinha, A. *et al.* The Asian monsoon over the past 640,000 years and ice age terminations. *Nature* **534,** 640–646 (2016).
19. Church, M. & Rood, K. Catalogue Of Alluvial River Channel Regime Data. The University of British Columbia, Department of Geography, Vancouver (1983).
20. Dalrymple, M., Prosser, J. & Williams, B. A dynamic systems approach to the regional controls on deposition and architecture of alluvial sequences, illustrated in the Statfjord Formation (United Kingdom, Northern North Sea). In: The Relative Role of Eustacy, Climate and Tectonism in Continental Rocks. *SEPM Special Publications* **59**, 65–81 (1998).
21. Densmore, A. L., Allen, P. A. & Simpson, G. Development and response of a coupled catchment fan system under changing tectonic and climatic forcing. *J. Geophy.s Res. Earth Surf.* **112**, (2007).
22. Dreyer, T. Quantified Fluvial Architecture in Ephemeral Stream Deposits of the Esplugafreda Formation (Palaeocene), Tremp-Graus Basin, Northern Spain. In: Alluvial Sedimentation (*Wiley*, 1993).
23. Fisher, J. A. & Nichols, G. J. Interpreting the stratigraphic architecture of fluvial systems in internally drained basins. *J Geol Soc London* **170**, 57–65 (2013).
24. Foreman, B. Z., Heller, P. L. & Clementz, M. T. Fluvial response to abrupt global warming at the Palaeocene/Eocene boundary. *Nature* 491, 92–95 (2012).
25. Gibling, M. R., Fielding, C. R. & Sinha, R. Alluvial Valleys and Alluvial Sequences: Towards a Geomorphic Assessment. In: From River to Rock Record: The preservation of fluvial sediments and their subsequent interpretation. *SEPM Special Publication* **97** (2011).

26. Greenberg, E., Ganti, V. & Hajek, E. Quantifying bankfull flow width using preserved bar clinoforms from fluvial strata. *Geology* **49**, 1038–1043 (2021).
27. Hajek, E. A. & Heller, P. L. Flow-Depth Scaling In Alluvial Architecture and Nonmarine Sequence Stratigraphy: Example from the Castlegate Sandstone, Central Utah, U.S.A. *J Sediment Res* **82**, 121–130 (2012).
28. Heard, T. G., Pickering, K. T. & Robinson, S. A. Milankovitch forcing of bioturbation intensity in deep-marine thin-bedded siliciclastic turbidites. *Earth Planet Sc. Lett.* **272**, 130–138 (2008).
29. Heller, P. L. & Paola, C. Downstream changes in alluvial architecture; an exploration of controls on channel-stacking patterns. *J. Sediment Res.* **66**, 297–306 (1996).
30. Holbrook, J., Scott, R. W. & Oboh-Ikuenobe, F. E. Base-Level Buffers and Buttresses: A Model for Upstream Versus Downstream Control on Fluvial Geometry and Architecture Within Sequences. *J Sediment Res.* **76**, 162–174 (2006).
31. Kelly, Sean. Scaling and hierarchy in braided rivers and their deposits: Examples and implications for reservoir modelling. In: Braided Rivers: Process, Deposits, Ecology and Management (*Wiley*, 2006).
32. Kjemperud, A.V., Schomacker, E., Brendsdal, A., Fält, L.M., Jahren, J., Nystuen, J.P., and Puigdefabregas, C. The Fluvial Analogue Escanilla Formation, Ainsa Basin, Spanish Pyrenees: Revisited. Search and Discovery Article, *AAPG International Conference*, Barcelona (2003).
33. Kodama, K. P., Anastasio, D. J., Newton, M. L., Pares, J. M. & Hinnov, L. A. High-resolution rock magnetic cyclostratigraphy in an Eocene flysch, Spanish Pyrenees. *Geochem. Geophys. Geosystems.* **11** (2010).
34. Labourdette, R. & Jones, R. R. Characterization of fluvial architectural elements using a three-dimensional outcrop data set: Escanilla braided system, South-Central Pyrenees, Spain. *Geosphere* **3**, 422–434 (2007).
35. Labourdette, R. Stratigraphy and static connectivity of braided fluvial deposits of the lower Escanilla Formation, south central Pyrenees, Spain. *AAPG Bulletin* **95**, 585–617 (2011).

36. Lane, E.W. The importance of fluvial morphology in hydraulic engineering. *Am. Soc. Civil Eng. Proc.* **81** (745), 1–17 (1955).

37. Leclair, S. & Bridge, J. Quantitative Interpretation of Sedimentary Structures Formed by River Dunes. *Journal of Sedimentary Research* **71,** 713–716 (2001).

38. Leeder, M. R., Harris, T. & Kirkby, M. J. Sediment supply and climate change: implications for basin stratigraphy. *Basin Res* **10**, 7–18 (1998).

39. Leopold, L. B., and Bull, W. B., 1979, Base level, aggradation, and grade. *Am. Philos. Soc. Proc.* **123**, 168–202 (1979).

40. Lyster, S. J. *et al.* Reconstructing the morphologies and hydrodynamics of ancient rivers from source to sink: Cretaceous Western Interior Basin, Utah, USA. *Sedimentology* **68**, 2854–2886 (2021).

41. Martinius, A.W., Elfenbein, C. and Keogh, K.J. Applying accommodation versus sediment supply ratio concepts to stratigraphic analysis and zonation of a fluvial reservoir. In: From Depositional Systems to Sedimentary Successions on the Norwegian Continental Margin (eds T. Stevens, A.W. Martinius, R. Ravnås, J.A. Howell, R.J. Steel and J.P. Wonham) (2014).

42. Michael, N. A., Whittaker, A. C., Carter, A. & Allen, P. A. Volumetric budget and grain-size fractionation of a geological sediment routing system: Eocene Escanilla Formation, south-central Pyrenees. *GSA Bulletin* **126**, 585–599 (2014).

43. Mohrig, D., Heller, P. L., Paola, C. & Lyons, W. J. Interpreting avulsion process from ancient alluvial sequences: Guadalope-Matarranya system (northern Spain) and Wasatch Formation (western Colorado). *GSA Bulletin* **112**, 1787–1803 (2000).

44. Noorbergen, L.J., Turtu, A., Kuiper, K.F., Kasse, C., Ginneken, S., Dekkers, M.J., Krijgsman, W., Abels, H.A., and Hilgen, F.J. Long-eccentricity regulated climate control on fluvial incision and aggradation in the Palaeocene of north-eastern Montana (USA). *Sedimentology* **67**, 2529–2560 (2020).

45. Ogg, J. & Ogg, G. & Gradstein, F. A Concise Geologic TimeScale (*Elsevier* 2016).

46. Olsen, H. Astronomical forcing of meandering river behaviour: Milankovitch cycles in Devonian of East Greenland. *Palaeogeography, Palaeoclimatology, Palaeoecology* **79**, 99–115 (1990).

47. Olsen, H. Orbital forcing on continental depositional systems - lacustrine and fluvial cyclicity in the Devonian of East Greenland. In: Orbital forcing and cyclic sequences (Wiley, 1994).

48. Paola, C. & Borgman, L. Reconstructing random topography from preserved stratification. *Sedimentology* **38**, 553-565 (1991).

49. Paola, C. & Mohrig, D. Palaeohydraulics revisited: Palaeoslope estimation in coarse-grained braided rivers. *Basin Res.* **8**, 243--254 (1996).

50. Parrish, J.T. Interpreting Pre-Quaternary Climate from the Geologic Record. (Columbia University Press, New York, 1998).

51. Posamentier, H.W. & Vail, P. Eustatic controls on clastic deposition II – Sequence and Systems Tract Models. In: Sea-Level Changes: An Integrated Approach. *SEPM Special Publication* **42** (1988).

52. Romans, B. W., Castelltort, S., Covault, J. A., Fildani, A. & Walsh, J. P. Environmental signal propagation in sedimentary systems across timescales. *Earth-sci Rev* **153**, 7–29 (2016).

53. Rush, W. D., Kiehl, J. T., Shields, C. A. & Zachos, J. C. Increased frequency of extreme precipitation events in the North Atlantic during the PETM: Observations and theory. *Palaeogeogr Palaeoclim Palaeoecol* **568**, 110289 (2021).

54. Schlager, W. Accommodation and supply—a dual control on stratigraphic sequences. *Sediment Geol* **86**, 111–136 (1993).

55. Schumm, S. A. River Response to Baselevel Change: Implications for Sequence Stratigraphy. *The Journal of Geology* ***101***, 279–294 (1993).

56. Shanley, K W, and McCabe, P J. Perspective on the sequence stratigraphy of continental strata. *AAPG Bulletin* **78** (1994).

57. Simpson, G. & Castelltort, S. Model shows that rivers transmit high-frequency climate cycles to the sedimentary record. *Geology* **40**, 1131–1134 (2012).

58. Sluijs, A., Zeebe, R. E., Bijl, P. K. & Bohaty, S. M. A middle Eocene carbon cycle conundrum. *Nat Geosci* **6**, 429–434 (2013).

59. Sun, T., Paola, C., Parker, G. & Meakin, P. Fluvial fan deltas: Linking channel processes with large-scale morphodynamics. *Water Resour Res*. **38**, 26-1-26–10 (2002).

60. Tofelde, S., Bernhardt, A., Guerit, L. & Romans, B. W. Times Associated With Source-to-Sink Propagation of Environmental Signals During Landscape Transience. *Frontiers Earth Sci* **9**, 628315 (2021).

61. Trampush, S. M., Huzurbazar, S. & McElroy, B. Empirical assessment of theory for bankfull characteristics of alluvial channels. *Water Resour Res.* **50**, 9211–9220 (2014).

62. Vallat, R. Pingouin: statistics in Python. *Journal of Open Source Software* **3** (2018).

63. Van den Berg Saparoea, V., & Postma, G. Control of climate change on the yield of river systems. SEPM Special Publication, 90 (2008).

64. Vinyoles, A. et al. 10 Myr evolution of sedimentation rates in a deep marine to non-marine foreland basin system: Tectonic and sedimentary controls (Eocene, Tremp–Jaca Basin, Southern Pyrenees, NE Spain). *Basin Res* (2020).

65. Wang, Y., Storms, J. E. A., Martinius, A. W., Karssenberg, D. & Abels, H. A. Evaluating alluvial stratigraphic response to cyclic and non-cyclic upstream forcing through process-based alluvial architecture modelling. *Basin Res* (2020).

66. Wolman, M. G. A method of sampling coarse river-bed material. *Eos Trans. AGU* **35**, 951– 956 (1954).

67. Wright, V. P. & Marriott, S. B. The sequence stratigraphy of fluvial depositional systems: the role of floodplain sediment storage. *Sediment Geol.* **86**, 203–210 (1993).

68. Zeebe, R.E., Westerhold, T., Littler, K., and Zachos, J.C. Orbital forcing of the Paleocene and Eocene carbon cycle. *Paleoceanography* **32**, 440–465 (2017).

69. Hajek, E. A., Heller, P. L. & Sheets, B. A. Significance of channel-belt clustering in alluvial basins. *Geology* **38**, 535–538 (2010).

70. Straub, K. M., Duller, R. A., Foreman, B. Z. & Hajek, E. A. Buffered, Incomplete, and Shredded: The Challenges of Reading an Imperfect Stratigraphic Record. *J Geophys Res Earth Surf* **125**, (2020).